MCSCF Study of Singlet Oxygen Addition to Ethenol—a Model of Photooxidation Reactions of Unsaturated and Aromatic Compounds Bearing Hydroxy Groups

ADAM LIWO,[1] DARIUSZ DYL,[2] DANUTA JEZIOREK,[2] MAŁGORZATA NOWACKA,[1] TADEUSZ OSSOWSKI,[1] WIESŁAW WOŹNICKI[2]*

[1]*Department of Chemistry, University of Gdańsk, Sobieskiego 18, 80-952 Gdańsk, Poland*
[2]*Institute of Physics, Nicholas Copernicus University, Grudziądzka 5, 87-100 Toruń, Poland*

Received 6 August 1996; accepted 18 April 1997

ABSTRACT: The reaction path of singlet ($^1\Delta_g$) oxygen addition to ethenol (vinyl alcohol)—a model of the reactions of singlet oxygen with aromatic and unsaturated compounds bearing the hydroxy groups—has been studied by means of MCSCF calculations, using various active spaces and basis sets. The effects of dynamic correlation (at the PT2 level) and basis set superposition error (BSSE) on relative energies were also investigated. It was found that including polarization functions is necessary to obtain geometries of the oxygen moiety consistent with the available experimental data. Two possible reaction products were considered: 1-hydroxy-1,2-dioxethane (peroxide) and 2-hydroperoxyethanal-1 (hydroperoxide); their energies are 24.1 and 36.6 kcal/mol (44.1 and 78.2 kcal/mol with the PT2 contribution and BSSE correction) below the dissociation limit, respectively (all energies reported here refer to the 6-31G** basis set and an active space composed of eight orbitals and ten electrons). A common stage of both reactions is the formation of a peralcoxyl intermediate with one of the oxygen atoms attached to the unsubstituted carbon atom; the energies of the respective transition state and that of the intermediate are 30.2 and 18.7 kcal/mol (15.9 and 10.3 kcal/mol with the PT2 contribution and BSSE correction) above the dissociation limit, respectively. The energy of this transition state is the dominant energy barrier to the reaction. The

* Deceased
Correspondence to: A. Liwo
Contract/grant sponsor: Polish State Committee for Scientific Research; contract/grant number: PB 0087/P3/93/05

This article includes Supplementary Material available from the authors upon request or via the Internet at ftp.wiley.com/public/journals/jcc/suppmat/18/1668 or http://journals.wiley.com/jcc/

CCC 0192-8651 / 97 / 131668-14

intermediate can then undergo conversion to the dioxethane product, to the perepoxide intermediate, or via a proton transfer, directly to the hydroperoxide, the last route being the most probable one. The perepoxide intermediate, after a proton transfer, also readily gives the hydroperoxide. It was also found that the unimolecular conversion from dioxethane to hydroperoxide via a proton transfer from the hydroxy group accompanied with ring cleavage requires an activation energy of at least 56 kcal/mol, making this reaction path highly improbable.
 J Comput Chem **18**: 1668–1681, 1997

Keywords: singlet oxygen; addition to double bond; hydroperoxides; MCSCF calculations

Introduction

Singlet ($^1\Delta_g$) oxygen addition to unsaturated and aromatic compounds plays an important role in living organisms. One of the main sources of this active oxygen species is the interaction of triplet $^3\Sigma_g$ oxygen with photoexcited triplet organic dye molecules.[1] Singlet oxygen addition to lipids and other unsaturated components of the living cells can directly initiate the chain of radical reactions leading to peroxidation,[3,4] whereas oxygen addition to xenobiotics can result in the generation of superoxide anion radicals and other active oxygen species of high cytotoxicity. Therefore, singlet oxygen can be involved in the photosensitivity of patients with erythropoietic protoporphyria[2] and drug photocytotoxicity.[3–7] Of particular importance are the reactions of singlet oxygen with conjugated and aromatic compounds bearing the hydroxy groups, such as anthraquinone derivatives, which are used as therapeutic anticancer agents.[8] In this case, oxygen addition is accompanied by a proton transfer from the hydroxy group to the attached oxygen molecule, which results in the formation of hydroperoxide ketones.[1,9–12] Moreover, allylic hydroperoxides are formed instead of peroxides when a methyl group, which is a much weaker proton donor than the hydroxy group, is attached to the carbon–carbon double (C=C) bond.[1,13,14] Some of the oxygen-addition reactions are schematically depicted in Figure 1.

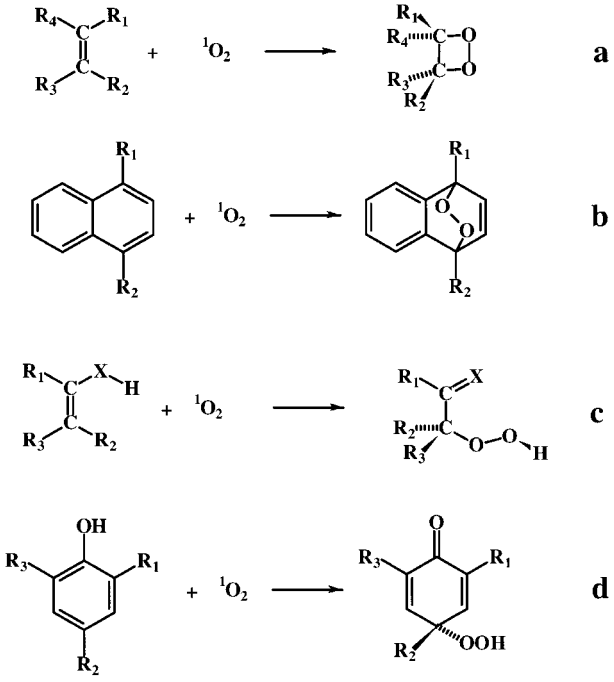

FIGURE 1. Examples of the reactions of oxygen addition to unsaturated and aromatic compounds: (a) 1,2 addition to olefins to form 1,2-dioxethane-type products; (b) 1,4 addition to nafthalene derivatives to form 1,4-endoperoxides; (c) 1,3 addition to olefin derivatives, X denotes CR_2, NR, or O; (d) addition to phenol derivatives containing bulky groups in position 2 and 4 of the ring form hydroperoxide ketones.

Photooxygenation reactions leading to the formation of dioxethanes have been a subject of extensive theoretical and experimental studies.[13–20] Three alternative mechanisms have been proposed: (i) a nonplanar $[2_s + 2_a]$ concerted addition[15,20] (Fig. 2a); (ii) a stepwise addition involving an acyclic peralcoxyl intermediate of biradicaloid or zwitterionic character[17] (Fig. 2b and c); and (iii) a stepwise addition through a largely zwitterionic perepoxide intermediate[15,17] (Fig. 2d). Based on the results of generalized valence bond (GVB) calculations, orbital-symmetry, and bond-energy analysis, as well as the regio- and stereoselectivity of the formation of dioxethanes and allylic peroxides, Harding and Goddard[14] concluded that the reaction most probably proceeds through the peralcoxyl intermediate; they predicted its character to be largely biradicaloid in the gas phase or

weakly polar solvents, and gradually more zwitterionic with increasing the polarity of the solvent. The unrestricted Hartree–Fock (UHF) *ab initio* and semiempirical MINDO/3 study by Yamaguchi et al.[21] confirmed that 1,4-biradicals are more stable than both the corresponding zwitterions and perepoxides, but those investigators noticed that this result contradicts the high stereospecificity and low regioselectivity of the photooxygenation reactions. Hotokka et al.[18] performed an extensive multi-configurational self-consistent field (MCSCF) and contracted configuration interaction (CCI) study of the possible modes of oxygen binding, using the double-ζ basis and the active space composed of eight orbitals with ten electrons. They concluded that the mechanism involving perepoxide intermediacy requires the lowest energy, although the intermediacy of the 1,4-biradical also is probable. Their conclusion regarding perepoxide intermediacy was, however, invalidated by the results of the most recent MCSCF study by Tonachini et al.,[22] who found that the putative transition state to perepoxide has two negative curvatures. The latter investigators' conclusion was that mechanism (ii), involving the 1,4-biradical intermediate (Fig. 2b), is the most probable one.

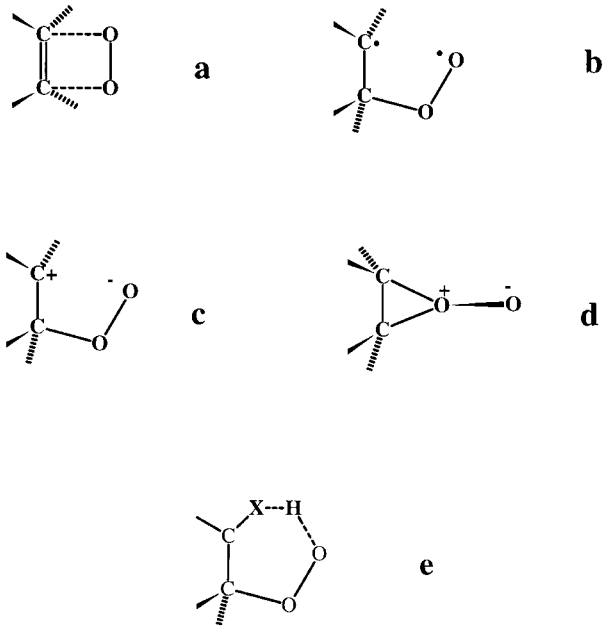

FIGURE 2. Proposed modes of oxygen binding to olefins: (a) concerted 1,2 addition; (b) formation of biradicaloid intermediate; (c) formation of zwitterionic intermediate; (d) formation of perepoxide intermediate; (e) conversion of zwitterionic or biradicaloid intermediate to allylic peroxide, hydroperoxide ketone, or hydroperoxide imine (with X = CR_2, NR, or O).

Compared to the formation of dioxethanes, there are many fewer reports in the literature on the theoretical studies of the formation of allylic hydroperoxides, hydroperoxide ketones, or hydroperoxide imines from unsaturated alcohols and amines and from phenols. In an early experimental report of oxygen addition to substituted phenols, Saito et al.[19] proposed peroxides to be intermediates, from which hydroperoxide ketones could be formed by a proton transfer accompanied with the C—O bond cleavage. The semiempirical MINDO/3 study of Dewar and Thiel[17] suggested that hydroperoxides can be formed from open zwitterionic or perepoxide intermediates by a proton transfer (Fig. 2e). The investigators also ruled out the possibility of the conversion of peroxides to hydroperoxides, as the energy barrier to this process is too high. However, their calculations were carried out with a closed-shell scheme and, therefore, the conclusions are valid only as long as the intermediates in the reaction can be considered single-configuration states; this may be incorrect in view of the results of the multiconfigurational studies of Tonachini et al.[22] and preceding workers.[14,18] In the aforementioned study,[14] Harding and Goddard suggested that allylic hydroperoxides can be formed from the 1,4-biradical intermediates by hydrogen-atom transfer from the neighboring carbon to the attached oxygen molecule (Fig. 2e).

In this article, we report the results of our *ab initio* MCSCF study of $^1\Delta_g$ oxygen addition to ethenol (vinyl alcohol), which may be regarded as the simplest model of the formation reaction of hydroperoxide ketones. (The species formed in this model reaction is 2-hydroperoxyethanol-1, which is actually a hydroperoxide aldehyde.) We investigated the reaction pathways leading to hydroperoxide and to dioxethane, as well as the possibility of proton transfer in dioxethane, resulting in its conversion to hydroperoxide aldehyde. The substrates and products of the reaction, together with the atom-designation system are shown in Figure 3.

Methods

To afford uniform treatment of the whole reaction path, calculations were carried out at the MCSCF level, with the 6-31G, 6-31 + G, 6-31G**, and double-ζ valence (DZV) basis sets. Two active

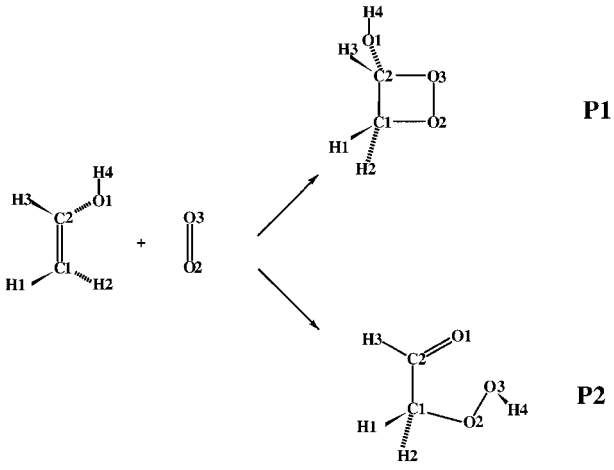

FIGURE 3. Substrates, dioxethane (P1), and hydroperoxide (P2) products of the reaction of singlet oxygen addition to vinyl alcohol.

spaces were implemented which consisted of 8 orbitals with 10 electrons and 10 orbitals with 12 electrons. They will hereafter be referred to as the (8,10) and (10,12) spaces, respectively. Calculations in the (10,12) active space were feasible only with the 6-31G basis set. The choice of the active space is discussed in the Results section. The main calculations were carried out with the GAMESS package,[23] whereas additional calculations to estimate the extent of dynamic correlation and basis set superposition error (BSSE) were carried out with using GAUSSIAN-94.[24]

The use of 6-31 + G basis set in part of the calculations was motivated by the fact that, according to earlier works,[14, 17, 18, 22] some of the stationary points on the reaction path (especially corresponding to the proton-transfer state) can be of highly zwitterionic character. Diffuse functions present in the 6-31 + G basis are designed to better describe the electronic state of a system bearing negative net charge or highly separated charge[25]; therefore, the protonation or proton-transfer energies calculated with the diffuse functions are lower and closer to experimental values than those calculated without diffuse functions. The polarization functions (6-31G** basis set) are often required to obtain reasonable valence geometry and bond energies.

The initial geometries of the substrates (ethenol and oxygen), intermediate I1, and the products hydroperoxide (P2) and dioxethane (P1) were constructed based on standard bond lengths and angles. The geometries of ethenol and the products were initially optimized at the restricted Hartree–Fock (RHF) level, with the 6-31G basis set. The optimized geometries were then taken as starting points to the optimization with the MCSCF wave function. Oxygen, intermediate I1, as well as the transition states and other stationary points in the reaction path that emerged during the course of this study, required multiconfigurational treatment from the beginning and, therefore, the minimal scheme to treat them was MCSCF with the (8,10) active space.

The transition states were localized by examining the variation of energy along the variable closest to the reaction coordinate (e.g., the C1 ⋯ O1 distance for the first stage of the reaction). After the approximate geometry of a transition state was obtained in such a way, the gradient-minimization (Sadpoint) option of GAMESS was used to calculate the exact geometry of the transition state. Final Hessian matrices were calculated for all minima and transition states, and their characteristics checked, to assure that the respective stationary points have the desired energy-surface curvature. Finally, intrinsic reaction coordinate (IRC) calculations were run from each of the transition states to check that they indeed lead to the energy minima between which they should be located.

For the optimized geometries of the stationary points on the reaction paths obtained with the 6-31G** basis set and the (8,10) active space, single-point MCSCF/PT2 calculations were carried out to estimate the extent of dynamic correlations. The correction for the basis set superposition error was also estimated in this calculation scheme, using the method developed by Chałasiński et al.[26] In this method, the energy of interaction of species A with species B in system A–B (it is assumed that the geometries of A and B can change on interaction) is first decomposed as follows:

$$\begin{aligned}\Delta E_{AB} &= E_{AB} - (E_A + E_B) \\ &= \left[E_{AB} - \left(\tilde{E}_A + \tilde{E}_B\right)\right] \\ &\quad + \left(\tilde{E}_A - E_A\right) + \left(\tilde{E}_B - E_B\right) \qquad (1)\end{aligned}$$

where E_A, E_B, and E_{AB} denote the energies of isolated A, isolated B, and the system A–B, respectively; $\tilde{E}_A$ denotes the energy of A at the geometry that it assumes in A–B, and $\tilde{E}_B$ denotes the energy of B at the geometry it has in A–B.

The terms $\tilde{E}_A - E_A$ and $\tilde{E}_B - E_B$ in eq. (1) can be regarded as the distortion energies of A and B

on the formation of A–B. They will not be influenced by the BSSE, because their components are calculated in the basis set of the same size. BSSE affects only the term $E_{AB} - (\tilde{E}_A + \tilde{E}_B)$. Because the distorted components have the same geometry as in A–B, the counterpoise procedure of Boys and Bernardi[27] can now be applied. Thus[26]:

$$\delta E_{A-B} = \left[\tilde{E}_A(\chi_A \cup \chi_B) - \tilde{E}_A(\chi_A) \right] + \left[\tilde{E}_B(\chi_A \cup \chi_B) - \tilde{E}_B(\chi_B) \right] \quad (2)$$

where χ_A and χ_B denote the basis sets of A and B and $\chi_A \cup \chi_B$ denotes the basis set of A–B. Thus, to estimate the BSSE four additional energy calculations are required: on subsystem A, in the geometry, it has in A–B with the basis set of A and with the basis set of A–B, respectively; and, on subsystem B, in the geometry, it has in A–B with the basis set of B and with the basis set of A–B, respectively.

Generally, the BSSE correction is considered to be overestimated in cases when the electron correlation is taken into account.[28] On the basis of the comparison of the calculated well-depths of the interaction potentials of the He_2, Ne_2, and He–Ne systems with the experimental data, Bachrach et al.[29] proposed to scale the correction of the interaction energy by the factor of 0.7. This procedure was implemented in our calculations.

Results and Discussion

CHOICE OF ACTIVE SPACE

To choose the minimum active space for the calculations, we based our data on the requirement that all orbitals and all electrons of the bonds being broken or formed should be included. Thus, the minimum requirement is to include the HOMO-LUMO $\pi_u 2p_z$C1–C2–$\pi_g^* 2p_z$C1–C2 pair of vinyl alcohol (z denoting the direction of the axis perpendicular to molecular plane) with two electrons [the (2,2) active space] and the $\pi_{2p_{\pm 1}}$–$\pi^*_{2p_{\pm 1}}$ bonding–antibonding pairs of the oxygen molecule with six electrons [the (4,6) active space][14, 18, 21, 22]; this constitutes the (6,8) active space for the whole system. Using this minimum active space with the aforementioned partition between oxygen and vinyl alcohol, we computed the energies of isolated substrates with the 6-31G basis set. For the $^1\Delta_g$ oxygen molecule, the energy in the (4,6) active space is −149.543581 a.u. (with optimized O—O bond length); the energy was averaged over the two components of the doubly degenerated $^1\Delta_g$ state. For vinyl alcohol, the RHF energy is −152.828076 a.u., and the energy computed with the (2,2) active space is −152.857480 a.u. (18.5 kcal/mol below the RHF energy). Extension of the active space of the oxygen molecule to (6,8) by incorporating the $\sigma_g 2p_o$–$\sigma_u^* 2p_o$ bonding–antibonding orbital pair results in lowering the energy to −149.612052 a.u.; that is, 43 kcal/mol, compared with the (4,6) space. This energy difference is larger than the energy difference of passing from the RHF energy of vinyl alcohol to the MCSCF energy computed in the (2,2) space, which suggests that the HOMO-LUMO orbitals of vinyl alcohol can be excluded from the active space to the favor of the inclusion of the $\sigma_g 2p_o$–$\sigma_u^* 2p_o$ orbitals of the oxygen molecule. In fact, we observed this undesirable feature of the solution to the MCSCF equations when trying to use the (6,8) space. To prevent this, we used the (8,10) space as the minimum active space; it includes both the $\sigma_g 2p_o$–$\sigma_u^* 2p_o$ orbitals of the oxygen molecule and the HOMO-LUMO pair of vinyl alcohol. The necessity of the incorporation of the $\sigma_g 2p_o$–$\sigma_u^* 2p_o$ pair was also pointed out by Hotokka et al.[18]

To examine the effect of extending the active space on the results, we also carried out calculations in the (10,12) space. For isolated reactants, this corresponds to the extension of the active space of vinyl alcohol to (4,4) by adding the $\sigma 2p$–$\sigma^* 2p$ bonding–antibonding orbital pair located mainly on the O1—H4 bond. The corresponding energy is −152.879161 a.u. [13.6 kcal/mol below the energy computed in the (2,2) space]. Extension of the active space of oxygen to (8,10) by incorporating the $\sigma_g 2s$–$\sigma_u^* 2s$ bonding–antibonding orbital pair results in lowering the energy only to −149.615927 a.u. [2.4 kcal/mol lower compared with the (6,8) space].

It should be noted that further extension of the active space of vinyl alcohol still resulted in significant lowering of the energy; therefore, even the most extensive (10,12) active space used in this work is far from saturated. Further extension of the active space for the whole system was, however, not feasible given the computational resource available. On the other hand, because all orbitals whose occupation changes most during the course of the reaction always remain within the active space, this deficiency is compensated for by the inclusion of dynamic correlation.

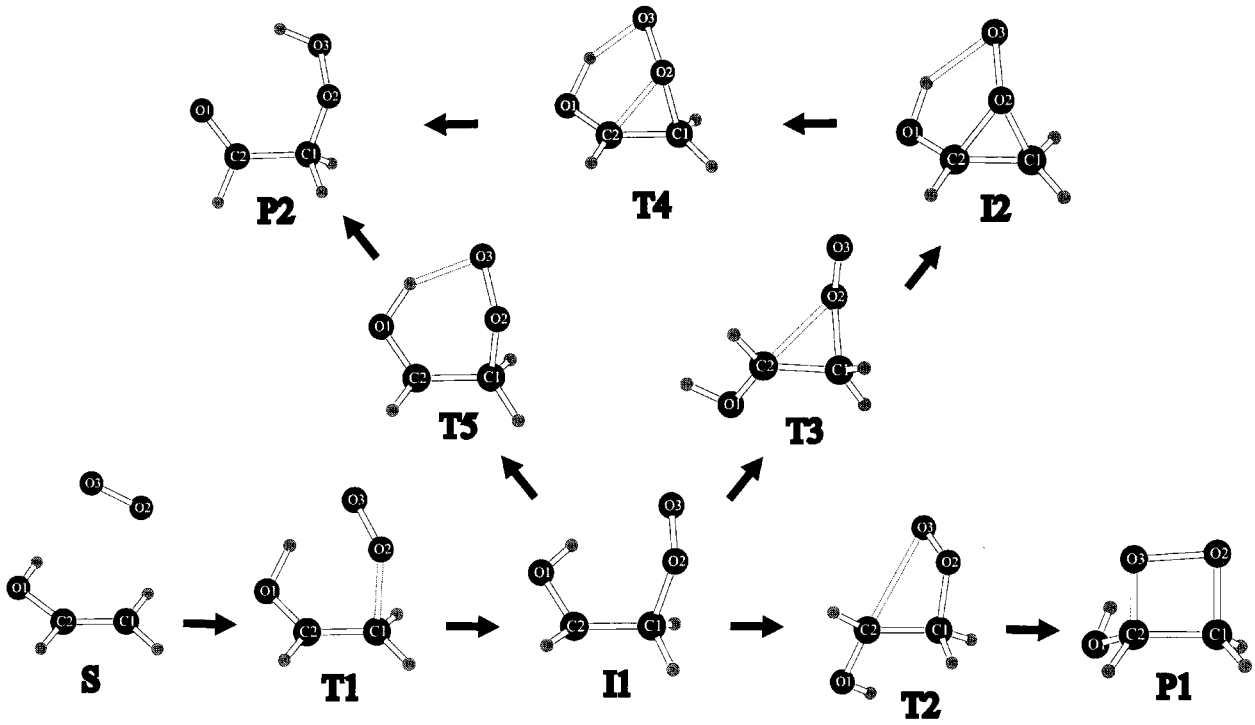

FIGURE 4. The structures of the stationary points on the reaction paths of singlet oxygen addition to vinyl alcohol. The geometries are optimized in the (8,10) / 6-31G** calculation scheme. S — isolated substrates; P1 — dioxethane product; P2 — hydroperoxide aldehyde product; I1 — peralcoxyl biradical intermediate; I2 — perepoxide intermediate; T1 — first transition state leading to the formation of I1; T2 — transition state leading from I1 to P1; T3 — transition state from I1 to I2; T4 — transition state from I2 to P2, T5 — transition state from I1 to P2.

MECHANISMS OF PEROXIDE AND HYDROPEROXIDE FORMATION

The complete reaction paths with all stationary points found are depicted in Figure 4 [at species geometries obtained in the (8,10)/6-31G** calculation scheme]. The relative energies of all the stationary points found on the reaction paths leading to hydroperoxide and dioxethane, computed in the (8,10) and (10,12) active spaces are summarized in Tables Ia and Ib. The relative energies of T1 and I1

TABLE Ia.
Total Energies of Substrates (Hartrees) and Relative Energies of Stationary Points in the Reaction Path of Oxygen Addition to Vinyl Alcohol (kcal / mol) Computed in All Active Spaces and Basis Sets Applied Except for the 6-31G Basis Set.**

	Scheme			
System[a]	6-31G (8,10)	6-31G (10,12)	6-31 + G (8,10)	DZV (8,10)
S	−302.469532	−302.491213	−302.480700	−302.542961
T1	26.46	22.19	25.96	27.48
I1	19.20	16.29	18.91	18.96
T2	25.53	18.55	25.76	25.69
P1	−18.53	−23.73	−18.16	−17.02
T3	23.00	18.69	24.61	27.09
I2	19.34	14.35	18.75	22.47
T4	23.75	18.37	23.90	27.37
P2	−33.76	−39.64	−26.95	−29.33

[a] See the legend to Figure 4 for explanations of the symbols of the species.

TABLE Ib.
Relative Energies and Amounts of Corrections for Dynamic Correlation (PT2 level) and Basis Set Superposition Error (kcal / mol) of Stationary Points on the Reaction Path Obtained Using the 6-31G Basis Set and the (8,10) Active Space.[a]**

Species[b]	ΔE_{MCSCF}[c]		$\Delta E_{MCSCF/PT2}$[d]			ΔE_2[e]	δE[f]	$\delta \Delta E_2$[g]
T1	30.21	32.37	9.19	15.90	13.89	−21.02	2.16	4.55
I1	18.69	21.36	1.93	10.33	7.81	−16.76	2.67	5.73
T2	26.18	28.84	−3.48	5.41	2.74	−29.66	2.66	6.23
P1	−24.14	−20.86	−57.05	−44.14	−48.01	−32.91	3.28	9.63
T3	33.76	36.31	19.42	28.75	25.95	−14.34	2.55	6.78
I2	15.63	18.50	−9.59	0.97	−2.20	−25.22	2.87	7.69
T4	17.92	20.79	−3.00	8.49	5.04	−20.92	2.87	8.62
T5	22.71	25.52	1.08	10.98	8.01	−21.63	2.81	7.09
P2	−36.56	−34.00	−87.50	−78.16	−80.96	−50.94	2.56	6.78

[a] All geometries were optimized at the MCSCF (8,10) / 6-31G** level and single-point calculations performed at the MCSCF (8,10) / 6-31G** / PT2 level. The sums of the total energies of substrates are −302.588945 and −303.230767 a.u. at the MCSCF and MCSCF / PT2 level, respectively.
[b] See legend to Figure 4 for explanations of the symbols of the species.
[c] MCSCF relative energies. Left column: uncorrected values; right column: BSSE-corrected values.
[d] MCSCF / PT2 relative energies. First column: uncorrected values; second column: values with full BSSE correction; third column: BSSE correction multiplied by the factor of 0.7, as in the work of Bachrach et al.[29]
[e] PT2 contribution to the relative energy.
[f] BSSE correction of the MCSCF energy.
[g] BSSE correction of the PT2 contribution to the relative energy.

obtained with the (8,10) active space are comparable with the energies of the corresponding stationary points of oxygen addition to ethene obtained by Tonachini et al.[22] with the (6,8) active space and the 4-31G basis set. Selected geometric parameters (except those involving the hydrogens bound to the carbon atoms) of the stationary points calculated with the (8,10) active space and the 6-31G and 6-31G** basis sets are shown and compared with available experimental data in Table II. Mulliken net atomic charges are summarized in Table III and the dominant configuration state functions (CSFs), as well as the occupation numbers and character of the natural orbitals of the active space are summarized in Table IV (see Fig. 3 for atom numbering).

As shown, the first stage of the reaction is the formation of a peralcoxyl intermediate, I1, which is analogous to that found in the theoretical studies of oxygen addition to ethylene.[14, 18, 22] Its formation occurs through the geometrically similar transition state T1. This transition state possesses a weak O1 ⋯ O3 hydrogen bond, which is absent in the intermediate I1. The latter fact can be attributed to a low net charge of the outermost oxygen atom O3 in I1 (Table III). Rotation about the C1—O2 bond can result in closing the four-membered ring to form dioxethane P1, through the quite open transition state T2. Intermediate I1 can also form the peroxirane intermediate I2 through the transition state T3, which ultimately, after the proton transfer from O1 to O3, gives the hydroperoxide P2. A simpler way to perepoxide P2 is a direct proton transfer in I1 through the transition state T5; this transition state was found only with the 6-31G** basis set.

The length of the O—O bond of the oxygen molecule calculated with the 6-31G basis set is too large compared to experiment (Table II). Extension of the active space to (10,12) does not change this. The agreement is better when using the 6-31 + G basis set, but the calculated O—O bond length of the singlet oxygen molecule (1.297 Å) is still quite different from the experimental value. Similar discrepancies between the calculated and experimental values of the O—O bond length occur for the dioxethane (P1) and hydroperoxide (P2) products, except that the latter is contained within the range of experimental values with the 6-31 + G basis set (1.446 Å). Other bond lengths, as well as the bond and torsional angles, agree well with the available experimental data in all calculation schemes. As

TABLE II.

Selected Bond Lengths and Other Interatomic Distances of Interest (Å), Bond Angles (deg.), and Dihedral Angles (deg.) of Stationary Points in the Reaction Paths Obtained in Calculations in (8,10) / 6-31G (A) and (8,10) / 6-31G (B) Calculation Schemes, Respectively.[a]**

	S			T1		I1		T2		P1		
Parameter	A	B	Exp.	A	B	A	B	A	B	A	B	Exp.
C1 — C2	1.338	1.335		1.385	1.381	1.471	1.480	1.498	1.505	1.502	1.510	1.48–1.552[c]
C2 — O1	1.381	1.353		1.358	1.295	1.371	1.346	1.377	1.348	1.390	1.366	
C1 — O2				1.896	1.793	1.540	1.481	1.500	1.447	1.541	1.471	1.432–1.51[c]
C2 ··· O2				2.394	2.228	2.439	2.388	2.349	2.289	2.196	2.099	
C2 — O3								2.467	2.364	1.524	1.415	
O2 — O3	1.309	1.240	1.2155[b]	1.409	1.349	1.447	1.349	1.512	1.396	1.674	1.530	1.44–1.505[c]
O1 — H4	0.951	0.944		0.962	0.991	0.952	0.945	0.952	0.945	0.953	0.946	
O3 ··· H4				2.074	1.631	2.349	2.288	3.780	3.676	2.529	2.435	
C1 — C2 — O1	125.8	126.3		120.9	120.9	119.1	118.1	118.8	119.2	116.5	117.7	
C2 — C1 — O2				92.4	88.1	108.2	107.5	103.1	101.6	92.4	89.5	
C1 — O2 — O3				108.1	109.6	107.4	108.8	99.1	99.8	85.5	88.0	
C1 — C2 — O3								65.4	64.0	92.4	90.9	
C2 — O3 — O2								67.5	69.6	86.6	90.8	
O1 — C2 — O3								138.7	142.3	111.4	112.8	
C2 — O1 — H4	115.0	110.6		115.5	107.8	116.3	111.7	115.6	111.0	113.8	109.7	
O3 — H4 ··· O1				130.6	143.3	117.8	116.2	73.0	73.6	71.8	71.5	
O1 — C2 — C1 — O2	−0.1	−0.1		75.4	72.6	65.2	61.9	−166.1	−168.6	−101.1	−109.9	
C2 — C1 — O2 — O3				−77.7	−73.5	−79.6	−80.7	53.4	53.1	−13.1	−6.1	
C1 — C2 — O1 — H4				−36.0	−41.2	4.2	12.7	52.3	46.4	61.3	55.8	
C1 — O2 — O3 — C2								−30.9	−32.1	12.9	6.5	
O2 — C1 — C2 — O3								−32.3	−31.2	14.3	6.6	

	T3		I2		T4		T5	P2		
Parameter	A	B	A	B	A	B	A	A	B	Exp.
C1 — C2	1.441	1.440	1.451	1.449	1.450	1.449	1.452	1.498	1.509	
C2 — O1	1.318	1.332	1.347	1.322	1.297	1.286	1.299	1.255	1.222	
C1 — O2	1.584	1.484	1.578	1.509	1.563	1.500	1.495	1.428	1.391	1.391–1.466[d]
C2 — O2	2.050	1.912	1.619	1.550	1.938	1.727				
O1 — O3	1.495	1.396	1.617	1.525	1.562	1.481	1.383	1.608	1.492	1.455–1.481[d]
O1 — H4	1.009	0.944	0.968	0.969	1.072	1.051	0.998			
O3 — H4	1.642	4.241	1.930	1.785	1.449	1.427	1.597	0.960	0.950	0.893–1.051[d]
C1 — C2 — O1	118.8	119.1	123.0	123.4	120.0	121.3	117.7	123.6	123.6	
C2 — C1 — O2	85.2	81.6	64.5	63.2	79.9	71.7	90.4	112.7	113.2	
C1 — C2 — O2	50.4	50.2	61.6	60.3	52.6	55.5	45.7	32.7	31.9	
C1 — O2 — C2	44.4	48.2	54.0	56.6	47.5	52.8	44.0	34.6	34.9	
C1 — O2 — O3	107.1	108.6	104.3	106.5	104.7	106.6	108.8	103.9	106.0	106.3–107.8[d]
O1 — C2 — O1	99.3	121.9	113.7	113.5	101.7	106.0	97.2	90.9	91.9	
O2 — O3 — H4					92.9	89.8		97.2	98.7	
C2 — O1 — H4	110.9	111.4	110.6	104.4	106.2	99.9	107.4	96.4	96.5	
O3 ··· H4 — O1	137.2	62.5	123.5	129.5	142.0	143.3	142.1	94.5	112.9	
O1 — C2 — C1 — O2	−77.5	−108.8	−101.2	−100.0	−81.6	−88.5	−71.7	3.1	5.3	
C2 — C1 — O2 — O3	82.9	−98.8	96.2	97.4	83.6	89.3	81.6	−71.8	−69.7	
C1 — C2 — O1 — H4	41.2	155.5	53.9	54.3	42.8	48.9	34.9			
C1 — O2 — O3 — H4								118.1	96.6	76.5–107.7[d]

[a] Experimental values of geometric parameters of similar compounds are shown where available in the third column corresponding to the respective species. See Figure 4 for explanations of the symbols of the species.
[b] Ref. 36.
[c] Ref. 37.
[d] Refs. 38–40.

TABLE III.
Mulliken Net Atomic Charges (Electron Charge Units) of Stationary Points in the Reaction Path Computed in the (8,10) / 6-31G (A) and (8,10) / 6-31G (B) Schemes.**

	S		T1		I1		T2		P1	
Atom	A	B	A	B	A	B	A	B	A	B
C1	−0.40	−0.35	−0.32	−0.22	−0.16	−0.02	−0.11	0.03	−0.09	0.02
C2	0.22	0.23	0.26	0.25	0.23	0.18	0.22	0.19	0.37	0.51
O1	−0.76	−0.62	−0.75	−0.61	−0.74	−0.59	−0.74	−0.60	−0.73	−0.62
O2	0.00	0.00	−0.13	−0.11	−0.25	−0.20	−0.31	−0.27	−0.31	−0.32
O3	0.00	0.00	−0.19	−0.21	−0.14	−0.19	−0.10	−0.14	−0.32	−0.37
H1	0.16	0.12	0.24	0.18	0.21	0.15	0.19	0.13	0.21	0.14
H2	0.17	0.13	0.21	0.17	0.22	0.16	0.21	0.15	0.21	0.14
H3	0.20	0.14	0.22	0.16	0.20	0.14	0.21	0.16	0.22	0.15
H4	0.41	0.34	0.45	0.37	0.44	0.36	0.42	0.35	0.43	0.35
DM[a]	1.78	1.28	2.64	3.97	2.93	2.61	2.79	2.78	2.89	2.58

	T3		I2		T4		T5	P2	
Atom	A	B	A	B	A	B	B	A	B
C1	−0.17	0.01	−0.13	−0.04	−0.15	−0.02	−0.02	−0.06	0.05
C2	0.30	0.24	0.36	0.44	0.34	0.40	0.25	0.26	0.30
O1	−0.73	−0.58	−0.73	−0.62	−0.72	−0.64	−0.60	−0.42	−0.42
O2	−0.21	−0.17	−0.31	−0.27	−0.27	−0.27	−0.18	−0.38	−0.36
O3	−0.40	−0.43	−0.43	−0.48	−0.47	−0.50	−0.38	−0.43	−0.36
H1	0.25	0.18	0.27	0.21	0.26	0.21	0.18	0.21	0.15
H2	0.23	0.19	0.23	0.18	0.23	0.17	0.17	0.22	0.15
H3	0.24	0.19	0.25	0.18	0.25	0.18	0.17	0.17	0.11
H4	0.49	0.37	0.48	0.41	0.53	0.47	0.41	0.44	0.38
DM[a]	4.58	3.73	4.77	4.49	5.28	4.67	4.48	2.79	2.84

[a]The dipole moment (D).

shown in Table II, agreement between the calculated and experimental values of the O—O bond lengths in all structures is reached only after including the polarization functions (Table II). Thus, as far as agreement with experimental data is concerned, the results obtained with the 6-31G** basis set should be considered the most reliable.

As mentioned previously, all calculation schemes except the (8,10)/6-31G** one give qualitatively the same reaction model, with the obligatory I2 perepoxide intermediate between I1 and P2. Conversely, whereas I2 was easily obtained as a true energy minimum with the 6-31G** basis set, in this calculation scheme we could not locate the transition state T3 (from I1 to I2), if the oxygen atom O3 was facing the H4 proton. Instead, the transition state T5 from I1 to P2 was always obtained. To locate the transition state T3, we had to rotate the O3 atom to the opposite side of the C2−C1−O2 plane. It can also be noted that the relative energy of T3 is higher, compared to those of the other transition states and intermediates than in the other computational schemes. The reason for this is probably the excessive O2—O3 bond length (by about 0.1 Å) obtained without the polarization functions. Thus, without the polarization functions, I1 has partially the character of a coordination compound between the alcoxyl biradical (composed of all atoms except O3) and the terminal oxygen atom O3 in the closed-shell ^{1}P state. This is manifested in the fact that the partial atomic charge of O3 in I1 is remarkably lower than that of O2 with the 6-31G basis set (Table III). Therefore, the O2 atom has more free valency than the O3 atom and the closing of epoxide ring occurs prior to proton transfer. Only after the epoxide ring is closed, the O3 atom develops enough negative charge for the proton transfer to occur.

By introducing the polarization functions, intermediate I1 can be considered as a peralcoxyl birad-

TABLE IV.
Dominant Configuration State Functions and Occupation Numbers of MCSCF Natural Orbitals Obtained in the (8,10) / 6-31G Scheme.**

	Natural orbital[a] (CSF)[b]									Natural orbital (occupation number)							
Species	1	2	3	4	5	6	7	8	Coeff.[b]	1	2	3	4	5	6	7	8
T1	2	2	2	2	2	0	0	0	0.94	2.00	1.98	1.96	1.94	1.89	0.16	0.06	0.02
	2	2	2	2	0	2	0	0	−0.31								
	2	2	2	0	2	0	2	0	−0.11								
I1	2	2	2	2	2	0	0	0	0.80	2.00	1.97	1.96	1.92	1.30	0.73	0.09	0.03
	2	2	2	2	0	2	0	0	−0.55								
T2	2	2	2	2	0	2	0	0	0.84	2.00	1.98	1.97	1.93	0.49	1.52	0.07	0.03
	2	2	2	2	2	0	0	0	−0.51								
	2	2	2	0	2	0	2	0	−0.12								
P1	2	2	2	2	2	0	0	0	0.96	2.00	2.00	1.96	1.86	1.98	0.02	0.14	0.04
	2	2	2	0	2	0	2	0	−0.20								
T3	2	2	2	2	2	0	0	0	0.93	2.00	1.99	1.96	1.95	1.92	0.08	0.05	0.04
	2	2	2	2	0	2	0	0	−0.25								
	2	1	2	1	2	1	1	0	−0.12								
	2	2	2	0	2	0	2	0	−0.12								
I2	2	2	2	2	2	0	0	0	0.97	2.00	2.00	1.96	1.94	1.96	0.04	0.06	0.05
	2	2	2	0	2	0	2	0	−0.14								
T4	2	2	2	2	2	0	0	0	0.96	2.00	2.00	1.96	1.95	1.92	0.06	0.08	0.04
	2	2	2	2	0	2	0	0	−0.10								
	2	2	2	0	2	0	2	0	−0.14								
T5	2	2	2	2	2	0	0	0	0.93	2.00	1.99	1.96	1.95	1.92	0.08	0.05	0.02
	2	2	2	2	0	2	0	0	−0.27								
	2	2	2	0	2	0	2	0	−0.12								
P2	2	2	2	2	2	0	0	0	0.96	2.00	2.00	1.98	1.87	1.93	0.07	0.13	0.02
	2	2	2	0	2	0	2	0	−0.20								
	2	2	2	2	0	2	0	0	−0.16								

[a]The approximate character of the subsequent natural orbitals is as follows: 3: $\sigma_g 2p_z$ C1 — O3. 4: $\sigma_g 2p_o$ O2 — O3. 5 and 6: $\pi^* 2p_y$ O2 — O3 $\pm$ $2p_z$ C2 (hereafter referred to as $b1$ and $b2$, respectively) in T1, I1, and T2; $\sigma_g 2p_z$ C2 — O3 and $\sigma_u^* 2p$ C2 — O3 in T3, I2, T4, and T5; $\sigma_g 2p_z$ C1 — O3 and $\sigma_u^* 2p_z$ C1 — O3 in P1; $\pi_u 2p_z$ C2 — O1 and $\pi_g^* 2p_z$ C2 — O1 in P2. 7: $\sigma_u^* 2p_o$ O2 — O3. 8: $\sigma_u^* 2p_z$ C1 — O3. Axis x follows the direction of the C1 — C2 bond, axis z follows the direction of the C2 — O3 bond, axis z is perpendicular to the C1 –O1 –O2 plane. The character of orbitals 1 and 2 varies between $\sigma 2s$ O2 — O3 — $\sigma^* 2s$ O2 — O3 and the $2p$ orbitals of O2 and O3, depending on species, even if the $2s$ orbitals of oxygen are excluded from the initial guess.

[b]Only the CSFs with coefficients greater than 0.1 in absolute value are shown.

ical rather than an alcoxyl–oxygen complex. The fact that comparable charge is localized on O2 and O3 (Table III) supports this observation. Therefore, the direct proton transfer from O1 to O3 can occur readily. Closing of the epoxide ring is less favorable in this case, because some electron density must be pushed toward O2. In conclusion, the model of the mechanism of hydroperoxide formation strongly depends on how well the O—O bond is accounted for by the calculation scheme used and the results obtained in the best calculation scheme used in this work [(8,10)/6-31G**] support the direct proton transfer in I1 rather than the intermediacy of perepoxide I2.

ENERGETICS OF OXYGEN ADDITION

All calculations carried out in this work clearly indicate that the hydroperoxide, P2, has much lower energy compared to the dioxethane, P1 (Tables Ia and Ib). We obtained the same result in earlier *ab initio* and semiempirical calculations on the energetics of oxygen binding by phenols and the hydroxy derivatives of 5,8-naphtoquinone and 9,10-anthraquinone.[30–32] The energies of the transition states from I1 to P1 (T2) and from I1 to P2 (T5) are comparable and thus the lower energy product, P2, should form, which is in agreement with experimental data of oxygen addition to unsatu-

rated and aromatic compounds with hydroxy groups.[1,9–12] Regardless of the calculation scheme, the formation of transition state T1 involves the highest energy; therefore, the relative energy of T1 can be considered the actual energy barrier to oxygen addition.

As shown in Table Ia, the estimated relative energies are lowered by several kilocalories per mole when the active space is increased. This means that the effect of the dynamic correlation on the relative energies might be significant. Table Ib contains the contributions of the dynamic correlation to the relative energies estimated using single-point PT2 calculations in the (8,10)/6-31G** scheme. It was not feasible to perform geometry optimization at this level of theory and therefore the estimated PT2 contributions can only be regarded as semiqualitative, which is illustrated by the fact that the PT2-corrected relative energies of T2 and T5 are below that of I1. As shown, the PT2 contributions are significant and amount to at least 16.8 kcal/mol. These contributions are, however, diminished when the BSSE correction is taken into account. In summary, the estimated barrier to oxygen addition (the energy of T1) ranges from 13 to 16 kcal/mol, depending on how the BSSE correction is scaled (the lower boundary was obtained using the scale factor of 0.7 developed by Bachrach et al.[29]). It can also be observed that the correlation contribution is much more affected by BSSE than MCSCF energy, a fact observed earlier by other workers.[28,29,33]

POSSIBILITY OF DIOXETHANE REARRANGEMENT TO HYDROPEROXIDE

Earlier works suggest that a unimolecular conversion from P1 to P2 through a proton transfer from O1 to O3 accompanied with the breaking of the C2—O3 bond is improbable, because of a large energy barrier.[14,16,17] To check whether high-level theoretical calculations support such a conclusion, we localized the direct transition state from P1 to P2 with the (8,10) active space and the 6-31G and 6-31 + G basis sets, respectively. Although this is not the best calculation scheme used in this work, it should be sufficient to compare the energy of this transition state with those of other transition states and intermediates in the reaction path. Moreover, the 6-31 + G basis set is able to handle its putatively high charge separation. The energies of the obtained transition state were 50.67 and 38.14 kcal/mol above the dissociation limit for the 6-31G and 6-31 + G basis sets, respectively. The corresponding barriers to the transition from P1 to P2 are 69.2 and 56.3 kcal/mol, which is in agreement with the calculated barriers to proton transfer of other unimolecular reactions reported in the literature (e.g., enol-ketone or iminol-amide tautomerization).[34,35] Even with the 6-31 + G basis set the energy of the direct transition state is still 13.5 kcal/mol higher than that of the I4 intermediate (which is highest in energy on the pathway from I1 to P2 in this calculation scheme). Thus, a more efficient way from P1 to P2 would be the opening of the dioxethane ring to form I1, with a subsequent proton transfer from O1 to O3.

CHANGES OF ELECTRONIC STRUCTURE DURING THE COURSE OF THE REACTION

A detailed discussion of the first stage of the oxygen-addition process has been given by Harding and Goddard.[14] The changes of the character and occupancy of the natural orbitals of the active space during the course of the reaction follow their considerations. In the initial phase of the reaction, the doubly occupied $\pi_u 2p_z$ orbital and the singly occupied $\pi_g^* 2p_z$ orbital of the oxygen molecule develop overlap with the $\pi_u 2p_z$ orbital of the vinyl alcohol to form the $\sigma_g 2p_z$ orbital of the C1—O2 bond (z denotes the direction of the C1—O2 axis). Because the last orbital comprises solely the C1 and O2 atoms, the empty $\pi_g^* 2p_z$ orbital of the C1—C2 bond also participates in its formation to zero out the coefficient at C2. The remaining part of the $\pi_u 2p_z - \pi_g^* 2p_z$ pair of the oxygen molecule forms the doubly occupied $2p_z$ orbital of the O3 atom. As a result, two approximately singly occupied orbitals, $b1$ and $b2$, are formed from the $2p_z$ orbital of the C2 carbon atom of the vinyl alcohol and the $\pi_g^* 2p_y$ orbital of the oxygen molecule, as shown in Figure 5. The two first of the dominant CSFs (Table IV) of the transition state T1 and intermediate I1 correspond to double occupation of either of these orbitals. The $\pi_u 2p_y$ orbital of the oxygen molecule remains almost intact both in T1 and I1; therefore, formally, only six electrons can be assigned to the outer O3 oxygen, which explains its low net charge in T1 and I1.

On bending the C2—C1—O2 angle of the intermediate I1, the orbital $b1$ develops overlap between its left $2p_y$ lobe of O2 and the upper $2p_z$ lobe of C2, to form the bonding $\sigma_g 2p$ orbital of the C2—O2 bond of the perepoxide intermediate I2 (Fig. 5); orbital $b2$ forms the corresponding antibonding $\sigma_u^* 2p$ orbital. The parts of $b1$ and $b2$ orbitals localized on the O3 atom and on the bond-

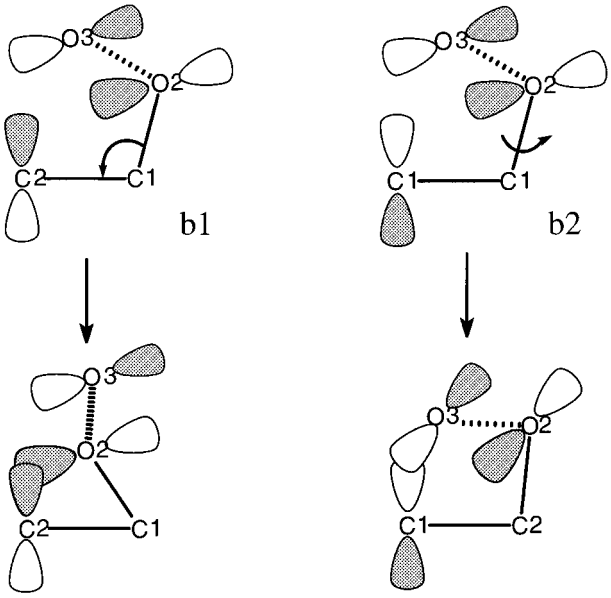

FIGURE 5. Schematic picture of the two outer singly occupied orbitals $b1$ and $b2$ of the biradical intermediate I1 (see text and Table IV for explanation) and the overlap of their parts leading to the $\sigma_g 2p_z$ C2 — O2 bonding orbital of dioxethane P1 or the $\sigma_g 2p_z$ C1 — O2 orbital of perepoxide intermediate I2.

ing $\pi_u 2p_y$ orbital are coverted into the doubly occupied $2p_y$ orbital of O3. Thus, the perepoxide intermediate, I2, is effectively in a closed-shell state (Table IV). The O3 oxygen atom formally acquires seven electrons, which explains its highly negative net charge (Table III). Further proton transfer from O1 to O3 involves the shift of the electron pair of the C2—O2 bond toward the O2 atom, while the freed $2p_z$ electron pair of the O1 oxygen atom spreads towards the now empty $2p_z$ orbital of the C2 atom, forming the π C2—O1 bond.

When the proton is transferred from the O1 to the O3 atom of I1, the resulting doubly filled $2p_z$ orbital of the O1 atom can develop overlap with the $2p_z$ orbital of the C2 atom (which is incorporated into the $b1$ and $b2$ orbitals of I1 and is, effectively, singly occupied), forming the $\pi_u 2p_z$–$\pi_g^* 2p_z$ bonding–antibonding orbital pair. However, this would leave one electron in the antibonding orbital and, at the same time, create electron deficiency in the O2—O3 moiety. Therefore, one electron is pushed towards the $\pi_g^* 2p_y$ O2—O3 part of the $b1$ and $b2$ orbitals, which, together with the participation of the doubly filled $\pi_u 2p_y$ orbital of the O2—O3 fragment, finally results in the formation of the doubly filled σ bonding orbital of the O3—H4 bond and the doubly filled $2p_y$ lone-pair orbital of the O2 atom of the hydroperoxide P2. This means that the rearrangement of I1 to P2 involves a hydrogen-atom transfer, rather than a proton transfer [it must be noted, however, that the $b1$ orbital has a greater occupation number than $b2$ (Table IV) and, therefore, the rearrangement does have a *partially* proton-transfer character]. Thus, in the case of 1,3 additions (cf. Fig. 1c) the X—H bond energy, rather than the proton affinity of the —X^- group should determine the barrier height to the rearrangement of the biradical intermediate to hydroperoxide. This explains why this rearrangement occurs readily even with the —CH_3 group, which has much worse proton-donor properties, compared to the —OH group.

On a rotation about the C1—O2 axis of I1, the second of the singly occupied $b1$ and $b2$ orbitals can develop overlap between the $2p_y$ part of the O3 outer oxygen and the $2p_z$ orbital of the C2 carbon atom, to form the bonding σ_g orbital of the C2—O3 bond, closing the four-membered ring. For this to occur, the nodal planes of those two $2p_z$ orbitals must initially be rotated.[14] When looking on the structure of the transition state T1 (Fig. 4), it can be noted that the C1H1H2 and the C2H3O1 groups are rotated by almost 90° about the C1—C2 axis, which forces the same rotation of the nodal planes of the $2p_z$ orbitals. In the transition state T2, the $b2$ orbital becomes more populated than $b1$, as opposed to the case of T1 and I1 (Table IV). Finally, in dioxethane P1 the orbital $b2$ is converted into the bonding σ_g orbital of the C2—O3 bond and the orbital $b1$ is converted into the corresponding antibonding orbital (Fig. 5).

It is interesting to note that the active space always comprises the $\sigma 2p_{og}$–$\sigma^* 2p_{ou}$ bonding–antibonding pair of the oxygen molecule and that the occupation numbers of these orbitals are apparently fractional (Table IV). The CSFs with the doubly occupied $\sigma^* 2p_{ou}$ orbital possess coefficients of 0.1 or larger in absolute value for all species. This is consistent with the remarkable energy lowering of the oxygen molecule after adding the $\sigma 2p_{og}$–$\sigma^* 2p_{ou}$ pair to the active space.

Conclusions

The results of our present study suggest that oxygen 1,3 addition to enols to form hydroperoxide ketones occurs in two stages: (i) the formation of a largely biradical peralcoxyl intermediate I1;

and (ii) a hydrogen-atom transfer (rather than a proton transfer) from the hydroxy group to the terminal oxygen atom. The last result indicates that the rearrangement of I1 will also occur via hydrogen-atom transfer in the case of oxygen 1,3 addition reactions to amino- and methyl-substituted double bonds, where the groups from which the proton or hydrogen atom must be abstracted have less pronounced proton-donor properties than the hydroxy group. A more complex route, involving the peroxirane intermediate I2 is also, in principle, possible; however, it requires more activation energy to form I2 from I1. Although this alternative route is not to be considered in the formation of hydroperoxide ketones *in vacuo* or in solvents with low polarity, it can be favorable in solvents with increased polarity, because the polar intermediate I2 can become stabilized in such conditions.[14]

Intermediate I1 can also convert to dioxethane P1, after closing the four-membered ring. The energy barrier to this reaction is comparable with that needed to form the hydroperoxide aldehyde P2; the product is, however, at least 10 kcal/mol higher in energy than P2. The estimated barrier to the direct proton transfer in P1 to form hydroperoxide ketone P2 in a unimolecular reaction is about 56 kcal/mol and therefore this possibility should be ruled out. On the other hand, such a reaction can probably occur in protic solvents, in which the solvent molecule can mediate the proton transfer.

The energy barrier to the first stage was calculated to be the dominant one and, therefore, this stage should be rate-determining. The estimated barrier amounts to about 13 to 16 kcal/mol after taking into account the dynamic-correlation contribution and the BSSE error, which is comparable with the experimental values of the energies of oxygen addition to unsaturated and conjugated compounds.[14]

Acknowledgments

The authors thank Prof. J. Wasilewski (Nicholas Copernicus University) for his thorough reading of the first draft of the manuscript and critical comments, as well as Dr. M. Gutowski (Pacific Northwest Laboratories) for his advice regarding MC-SCF calculations. This work was supported by grant No. PB 0087/P3/93/05 from the Polish State Committee for Scientific Research (KBN). The calculations were carried out on the Cray YMP/4E and Power Challenge SGI R-10000 computers at the Interdisciplinary Center for Mathematical Modeling at Warsaw University; the Power Challenge SGI R-10000 computer at the Informatics Center of the Metropolitan Academic Network (IC MAN) at the Technical University of Gdańsk; and the RS 6000 and Sun Sparc Classic V workstations at the Institute of Physics of Nicholas Copernicus University, Toruń, and the Department of Chemistry of the University of Gdańsk, respectively.

References

1. E. A. Lissi, M. Encinas, E. Lemp, and M. A. Rubio, *Chem. Rev.*, **93**, 699 (1993).
2. M. M. Matthews-Roth, In *The Science of Photomedicine*, J. D. Regan and J. A. Parish, Eds., Plenum Press, New York, 1982, p. 409.
3. B. Halliwell and J. M. C. Gutteridge, *Free Radicals in Biology and Medicine*, Clarendon Press, Oxford, 1985.
4. W. A. Pryor, Ed., *Free Radicals in Biology, Vol. V*, Academic Press, New York, 1982.
5. D. E. Moore, V. J. Hemmens, and H. Yip, *Photochem. Photobiol.*, **39**, 57 (1984).
6. R. W. Tuveson, G. R. Wang, T. P. Wang, and J. Kagan, *Photochem. Photobiol.*, **52**, 993 (1990).
7. C. Thomas, R. S. MacGill, G. C. Miller, and R. S. Pardini, *Photochem. Photobiol.*, **55**, 47 (1992).
8. J. W. Lown, *Chem. Soc. Rev.*, 165 (1993).
9. F. Jensen and C. S. Foote, *Photochem. Photobiol.*, **46**, 325 (1987).
10. M. S. Kharasch and B. S. Joshi, *J. Org. Chem.*, **22**, 1439 (1957).
11. M. J. Thomas and C. S. Foote, *Photochem. Photobiol.*, **27**, 683 (1978).
12. P. Dowd, S. W. Ham, and S. J. Geib, *J. Am. Chem. Soc.*, **113**, 7734 (1991).
13. C. W. Jefford, *Chem. Soc. Rev.* 59 (1993), and references therein.
14. L. B. Harding and W. A. Goddard III, *J. Am. Chem. Soc.*, **102**, 439 (1980).
15. D. R. Kearns, *Chem. Rev.*, **71**, 395 (1971).
16. A. A. Frimer, *Chem. Rev.*, **79**, 359 (1979).
17. M. J. S. Dewar and W. Thiel, *J. Am. Chem. Soc.*, **97**, 3978 (1975).
18. M. Hotokka, B. Roos, and P. Siegbahn, *J. Am. Chem. Soc.*, **105**, 5263 (1983).
19. I. Saito, S. Kato, and T. Matsuura, *Tetrahed. Lett.*, 239 (1970).
20. P. D. Bartlett and A. P. Schaap, *J. Am. Chem. Soc.*, **92**, 3223 (1970).
21. K. Yamaguchi, S. Yabushita, T. Fueno, and K. N. Houk, *J. Am. Chem. Soc.*, **103**, 5043 (1981).
22. G. Tonachini, H. B. Schlegel, F. Bernardi, and M. A. Robb, *J. Am. Chem. Soc.*, **112**, 483 (1990).
23. M. W. Schmidt, K. K. Baldridge, J. A. Boatz, S. T. Elbert, M. S. Gordon, J. J. Jensen, S. Koseki, N. Matsunaga, K. A. Nguyen, S. Su, T. L. Windus, M. Dupuis, and J. A. Montgomery, *J. Comput. Chem.*, **14**, 1347 (1993).

24. M. J. Frisch, G. W. Trucks, H. B. Schlegel, P. M. W. Gill, B. G. Johnson, M. A. Robb, J. R. Cheeseman, T. Keith, G. A. Petersson, J. A. Montgomery, K. Raghavachari, M. A. Al-Laham, V. G. Zakrzewski, J. V. Ortiz, J. B. Foresman, J. Cioslowski, B. B. Stefanov, A. Nanayakkara, M. Challacombe, C. Y. Peng, P. Y. Ayala, W. Chen, M. W. Wong, J. L. Andres, E. S. Replogle, R. Gomperts, R. L. Martin, D. J. Fox, J. S. Binkley, D. J. Defrees, J. Baker, J. P. Stewart, M. Head-Gordon, C. Gonzalez, and J. A. Pople, *GAUSSIAN-94, Rev. D.4*, Gaussian, Inc., Pittsburgh, PA, 1995.
25. W. J. Hehre, L. Radom, P. R. von Schleyer, and J. A. Pople, *Ab Initio Molecular Orbital Theory*. John Wiley & Sons, New York, 1986, p. 86.
26. G. Chałasiński, R. A. Kendall, and J. Simons, *J. Chem. Phys.*, **87**, 2965 (1987).
27. S. J. Boys and F. Bernardi, *Mol. Phys.*, **19**, 553 (1970).
28. S. Saebø and W. Tong, *J. Chem. Phys.*, **3**, 2170 (1993).
29. S. M. Bachrach, R. A. Chiles, and C. E. Dykstra, *J. Chem. Phys.*, **75**, 2271 (1981).
30. D. Jeziorek, D. Dyl, A. Liwo, T. Ossowski, and W. Woźnicki, *Anti Cancer Drug Design*, **9**, 435 (1994).
31. A. Liwo, D. Jeziorek, T. Ossowski, D. Dyl, A. Tempczyk, J. Tarasiuk, M. Nowacka, E. Borowski, and W. Woźnicki, *Acta Biochim. Pol.*, **42**, 445 (1995).
32. D. Jeziorek, T. Ossowski, A. Liwo, D. Dyl, M. Nowacka, and W. Woźnicki, *J. Chem. Soc. Perkin Trans.* **II**, 229 (1997).
33. R. A. Kendall, J. Simons, M. Gutowski, and G. Chałasiński, *J. Phys. Chem.*, **93**, 621 (1989).
34. A. L. Sobolewski, *J. Photochem. Photobiol. A*, **89**, 89 (1995).
35. C.-C. Wu and M.-H. Lien, *J. Phys. Chem.*, **100**, 594 (1996).
36. G. Herzberg, *Molecular Spectra and Molecular Structure. I. Spectra of Diatomic Molecules*, Van Nostrand, New York, 1950.
37. W. Adam, L. A. Arias, A. Zahn, K. Zinner, K. Peters, E.-M. Peters, and H. G. von Schnering, *Tetrahed. Lett.*, **23**, 3251 (1982).
38. A. G. Nord and B. Lindberg, *Acta Chem. Scand.*, **27**, 1175 (1973).
39. B. Carte, M. R. Kernan, E. B. Barrabee, D. J. Faulkner, G. K. Matsumoto, and J. Clardy, *J. Org. Chem.*, **51**, 3528 (1986).
40. G. Bernardinelli, C. W. Jefford, J. Boukouvalas, D. Jaggi, and S. Kohmoto, *Acta Crystallogr. C*, **43**, 701 (1987).